

Article

# Iterative 2D Tissue Motion Tracking in Ultrafast Ultrasound Imaging

John Albinsson <sup>1</sup>, Hideyuki Hasegawa <sup>2</sup>, Hiroki Takahashi <sup>2</sup>, Enrico Boni <sup>3</sup> ,  
Alessandro Ramalli <sup>3,4</sup> , Åsa Rydén Ahlgren <sup>5,6</sup> and Magnus Cinthio <sup>1,\*</sup> 

<sup>1</sup> Department of Biomedical Engineering, Faculty of Engineering, Lund University, 221 00 Lund, Sweden; john.albinsson@bme.lth.se

<sup>2</sup> Graduate School of Science and Engineering for Research, University of Toyama, Toyama 930-8555, Japan; hasegawa@eng.u-toyama.ac.jp (H.H.); takahashi.hiroki@xpost.plala.or.jp (H.T.)

<sup>3</sup> Department of Information Engineering, University of Florence, 501 39 Florence, Italy; enrico.boni@unifi.it (E.B.); alessandro.ramalli@unifi.it (A.R.)

<sup>4</sup> Laboratory of Cardiovascular Imaging and Dynamics, Department of Cardiovascular Sciences, KU Leuven, 3000 Leuven, Belgium

<sup>5</sup> Department of Translational Medicine, Lund University, 221 00 Lund, Sweden; asa.ryden\_ahlgren@med.lu.se

<sup>6</sup> Department of Medical Imaging and Physiology, Skåne University Hospital, Lund University, 205 02 Malmö, Sweden

\* Correspondence: magnus.cinthio@bme.lth.se; Tel.: +46-(0)46-222-9710

Received: 7 March 2018; Accepted: 21 April 2018; Published: 25 April 2018



**Abstract:** In order to study longitudinal movement and intramural shearing of the arterial wall with a Lagrangian viewpoint using ultrafast ultrasound imaging, a new tracking scheme is required. We propose the use of an iterative tracking scheme based on temporary down-sampling of the frame-rate, anteroposterior tracking, and unbiased block-matching using two kernels per position estimate. The tracking scheme was evaluated on phantom B-mode cine loops and considered both velocity and displacement for a range of down-sampling factors ( $k = 1$ –128) at the start of the iterations. The cine loops had a frame rate of 1300–1500 Hz and were beamformed using delay-and-sum. The evaluation on phantom showed that both the mean estimation errors and the standard deviations decreased with an increasing initial down-sampling factor, while they increased with an increased velocity or larger pitch. A limited in vivo study shows that the major pattern of movement corresponds well with state-of-the-art low frame rate motion estimates, indicating that the proposed tracking scheme could enable the study of longitudinal movement of the intima–media complex using ultrafast ultrasound imaging, and is one step towards estimating the propagation velocity of the longitudinal movement of the arterial wall.

**Keywords:** ultrafast ultrasound imaging; block-matching; speckle tracking; arterial longitudinal wall movement; in vivo

## 1. Introduction

Ultrafast ultrasound imaging has been used as the basis for the development of a number of methods intended for diagnosing and exploring different phenomena in vivo, e.g., shear wave elastography [1–4], acoustic radiation force impulse imaging [5], vector flow imaging [6–8], and a method for skeletal muscle contraction [9], functional ultrasound imaging of the brain [10], and cardiac motion [11,12]. The arterial walls have been investigated by estimating the radial strain in the common carotid artery [13] and the radial pulse wave velocity [14,15].

In cardiovascular research, the radial movement of the arterial wall, i.e., the diameter change, has been the subject of extensive research, forming the basis for estimation of arterial wall stiffness [16]. Increased stiffness of the large central arteries has been shown to be an independent risk factor for cardiovascular mortality [17]. In contrast to the radial movement, the longitudinal movement of the arterial wall has gained less attention. We have, however, shown that in both large predominantly elastic arteries and in large muscular arteries there is a distinct bi-directional displacement of the arterial wall during the cardiac cycle [18]. The intima–media of these arteries exhibits a longitudinal displacement that is larger than that of the adventitial region [18] and thus, there is shear strain and shear stress within the arterial wall [18–21]. We have recently reported that longitudinal movement and intramural shear strain undergo profound changes in response to the important circulatory hormones adrenalin and noradrenalin [22], indicating that the longitudinal movements and resulting intramural shear strain can constitute an important but overlooked mechanism in the cardiovascular system. Studies have indicated that the maximal amplitude of the longitudinal displacement of the common carotid artery is reduced in subjects with cardiovascular risk factors [23], and suspected and manifest atherosclerotic disease [24,25]. However, the physiology behind the observed longitudinal vessel wall movement pattern is largely unknown.

It is our belief that the use of ultrafast ultrasound imaging in combination with 2D tissue motion estimation can increase our understanding of this phenomenon and make it possible to estimate the propagation velocity of the longitudinal movement. However, to explore the longitudinal movement of the arterial wall by using ultrasound, the artery is scanned in the longitudinal direction and the longitudinal movement of the arterial wall occurs in the lateral direction of the ultrasound image. It is problematic to estimate lateral tissue motion in ultrafast ultrasound imaging *in vivo* as the tissue moves only a very short distance between consecutive frames due to the high frame rate. Thus, the motion to be estimated will be very small compared to the expected uncertainty in the motion estimates caused by the limited signal-to-noise ratio. The estimation uncertainty is larger in the lateral direction [26] as ultrasound frames normally have lower spatial resolution in the lateral direction. Consequently, Lagrangian tracking in the lateral direction and in every frame is very likely to give a large accumulated error even with an unbiased motion estimator when using ultrafast ultrasound imaging. The motion estimations can be improved by averaging motion estimations over multiple frames, but this will decrease the effective frame rate and will function as a low-pass filter on the motion estimations in the time domain. This can potentially hide vital information in the motion estimations.

In this paper, we propose to estimate 2D motions with a Lagrangian viewpoint in ultrafast ultrasound cine loops using an iterative motion estimation tracking scheme in which the initial length between the used frames is larger than one. Contrary to phase-sensitive motion estimation methods (e.g., [14,27]) where the estimated motion must be small to avoid aliasing, our experience shows that the relative motion estimation error decreases for block-matching methods when the length of the estimated motion increases [26]. Since the motion between two frames in ultrafast ultrasound cine loops is often very small and the speckle decorrelation is limited, the risk for the speckle decorrelation over several, e.g., 128, frames is small but the total motion over this number of frames will be larger and easier to accurately estimate using block-matching. Therefore, we propose a temporary down sampling of the frame rate in which a first Lagrangian motion estimation is performed between each  $k$  frame, e.g., initial frame interval  $k = 128$ . The cine loop is thereafter iteratively re-sampled with shorter frame intervals and the position of the kernel in one in-between frame can be estimated using the two kernels of the anteroposterior frames as reference kernels. The tracking scheme is hypothesized to reduce the size of the accumulative errors both by using two separate motion estimations for each estimated position, thus reducing each estimation error, and by using much fewer estimations from the start of the tracking before reaching the investigated frame.

The aim of this study was to evaluate the proposed 2D tissue motion estimation tracking scheme in ultrafast ultrasound cine loops. In a phantom evaluation, the proposed tracking scheme was evaluated for a range of initial down-sampling factors ( $k = 1–128$ ). The motion estimation errors of the

proposed tracking scheme using ultrafast ultrasound cine loops were compared to those obtained in low frame rate cine loops, obtained with conventional beamforming. The motion estimation errors of both velocity and displacement were evaluated. The tracking performance was evaluated using a 100  $\mu\text{m}$  pitch transducer and a 200  $\mu\text{m}$  pitch transducer. The feasibility of using the proposed 2D tissue motion estimation tracking scheme in vivo was evaluated in a limited in vivo study.

## 2. Materials and Methods

The in-house block-matching method, developed to estimate the location of the target in a given frame, builds on works by Albinsson et al. [26,28] and will be summarized below. Here, we propose a novel tracking scheme that is based on the re-sampling of the cine loop along the time axis. The tracking performance of the novel 2D tissue motion estimator was evaluated on phantom and in vivo cine loops. Furthermore, the tracking performance obtained in ultrafast cine loops was compared to that achieved in low frame rate cine loops, obtained with conventional beamforming.

### 2.1. Proposed Tracking Scheme

The method denoted as the “basic method” in [28] is a sparse iterative block-matching method, that uses the sum of absolute differences as the matching criterion and an unlimited search area. In this work, the sub-sample method has been replaced with the method presented below. The method denoted “basic method using an extra reference block” in [28] uses two independent kernels from two consecutive frames. The search area of the second kernel is limited to a small area around a position determined by the “basic method”.

The proposed motion estimation tracking scheme consists of two parts:

1. First, the frame rate is temporarily down sampled by a factor  $k$ , where  $k = (2, 4, 8, 16, 32, 64, \text{ or } 128)$ . The position of each kernel is estimated with a Lagrangian viewpoint between every frame in the temporary cine loop (solid lines in Figure 1a). The position of the kernel in each frame is estimated using a block-matching method with an extra kernel described in [28] (where the method is denoted as the “basic method using an extra reference block”). This method was developed to minimize estimation errors when using a Lagrangian viewpoint.
2. Iteratively: the frame rate is temporarily down sampled by a factor  $m = k/2^i$  where  $i$  is the iteration number. The unknown kernel positions in each middle frame in the temporary cine loop are determined by the kernels from the anteroposterior frames (dashed lines in Figure 1b). The two independently estimated positions are averaged to determine the kernel position in the middle frame. The iterations continued until the position of the kernel is estimated in every frame (dashed lines in Figure 2c), i.e.,  $m = 1$ . The position of the kernel is estimated using the block-matching method denoted “basic method” in [28].

The sub-sample estimation in both part 1 and 2 is first performed by parabolic interpolation; if the estimate is  $y \pm 0.15$  pixels, where  $y$  is any natural number, the estimate is used, otherwise a modified grid slope sub-sample estimator is used to recalculate the estimate [26]. Parabolic and grid slope interpolation complement each other: parabolic interpolation is biased for sub-sample estimation close to  $y \pm 0.5$  pixels, whereas grid slope interpolation gives noisy estimates close to  $y \pm 0.0$  pixels.

The size of a kernel in the phantom study was 1 mm axially and laterally. This resulted in an axial kernel size of 41 pixels, and a lateral kernel size of 11 pixels using 100  $\mu\text{m}$  line distance and 5 pixels using 200  $\mu\text{m}$  line distance. The size of a kernel in the in vivo study was 0.6 mm axially and 3.8 mm laterally.

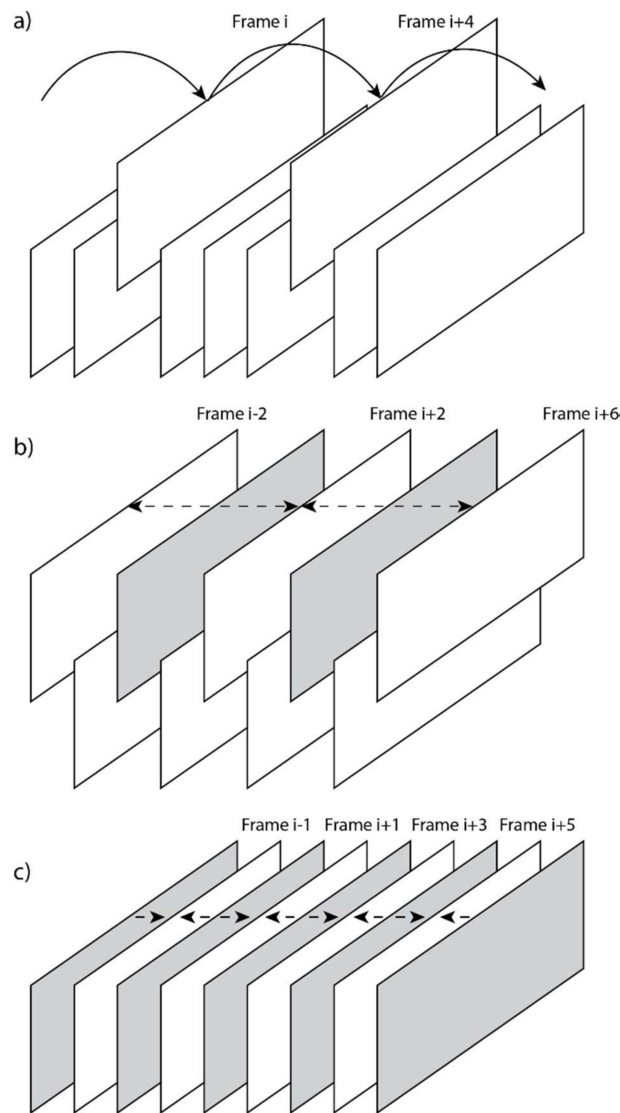


**Figure 1.** The figure shows which frames to use in (a) part 1 and (b,c) part 2 (1st and 2nd iteration) of the proposed tracking scheme for  $k = 4$ . The squares mark sampled frames and a raised frame marks a frame used in the current iteration. Please note that all frames are raised in (c) (2nd iteration). A gray frame marks a frame in which a position for the kernel has been estimated in a previous iteration. The base of the arrows shows the frame in which the kernel is collected and the point of the arrows shows in which frame the kernel is searched for. In (b,c) iteration, there are two arrows pointing at each frame in which to estimate the position. The estimated position in these frames is calculated as the average estimated position using two kernels from two different frames.

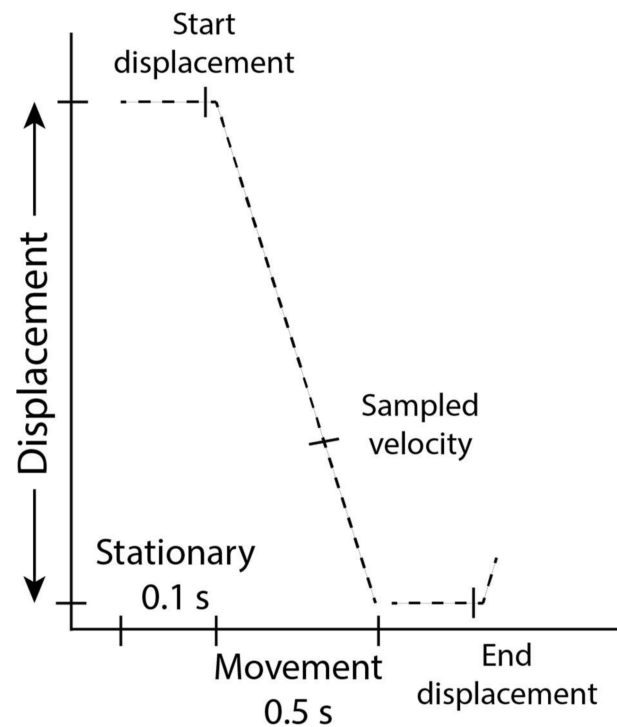


**Figure 2.** Scheme for the set motion of the transducer and the frames used for determining displacement and velocity. The displacement of each kernel was calculated as the difference between its position in the start and end frames. The velocity was estimated as the difference between two consecutive frames.

## 2.2. Cine Loops

The phantom cine loops were collected in Japan at a pulse repetition frequency of 5208 Hz by a 96-channel ultrasound scanner (RSYS0002, Microsonic, Tokyo, Japan) equipped with two linear array ultrasonic transducers with a center frequency of 7.5 MHz. The transducers had a pitch of 100  $\mu\text{m}$  and 200  $\mu\text{m}$ , respectively, which corresponds to  $\lambda/2$  and  $\lambda$ . The pixel densities in the cine loops were 40.6  $\text{mm}^{-1}$  axially and either 10.0  $\text{mm}^{-1}$  or 5.0  $\text{mm}^{-1}$  laterally depending on the pitch of the transducer. Each transducer was moved diagonally repeatedly back and forth at constant velocity with short stops at each turning point (Figure 2) using automatic stages (ALS-6012-G0M and ALV-600H0M, Chuo Precision Industrial, Tokyo, Japan). A sponge was used to create realistic speckle. Two different velocities were used: 2.0 mm/s laterally and 1.0 mm/s axially with displacements of 1.0 mm laterally and 0.5 mm axially; and 1.0 mm/s laterally and 0.5 mm/s axially with displacements of 0.5 mm laterally and 0.25 mm axially. In the lateral direction, this corresponds to a displacement of 1.5  $\mu\text{m}/\text{frame}$  and 0.77  $\mu\text{m}/\text{frame}$ , respectively. The collected radio frequency data were beamformed using delay-and-sum [13]. In the present study, one frame was obtained from four plane wave transmissions resulting in a frame rate of 1302 Hz. A plane wave is transmitted with 96 active elements, and echo signals were received by the same elements. Each receiving beam was created using the echo signals obtained from 72 of 96 elements. Consequently, 24 receiving beams were created in one transmit event. Then, the active aperture was translated laterally by 24 elements, and the same procedure was repeated four times to obtain 96 receiving beams. In receive, a Hanning apodization was used. Cine loops were also collected at a lower frame rate (41 Hz) with a conventional linear scan scheme. These cine loops used the same transducers, transducer movements, and kernel size, while the motion estimations were conducted in every frame ( $k = 1$ , see above).

To evaluate the feasibility of using the proposed 2D tissue motion estimation tracking scheme in vivo, a limited in vivo study was conducted in Sweden. The in vivo experiment was performed using a 64-channel ULA-OP system [29,30] equipped with a 192-element LA435 linear array transducer

(Esaote SpA, Florence, Italy) with a 200  $\mu\text{m}$  pitch. The cine loops were collected at 1500 Hz using a single plane wave transmission; the 64-line frames were beamformed using delay-and-sum with dynamic apodization having the f-number equal to 2. The line distance between the 64 lines was 200  $\mu\text{m}$ . ECG was not available. To be able to compare with state-of-the-art estimation of the longitudinal movement of the arterial wall, low frame rate cine loops in vivo were collected using a Philips Epiq 7 (Philips Medical Systems, Bothell, WA, USA) equipped with a linear array transducer (model L18-5, Philips Medical Systems, Bothell, WA, USA). The right common carotid artery was scanned in the longitudinal direction, oriented horizontally in the image 2–3 cm proximal to the bifurcation. The healthy volunteers gave informed consent according to the Helsinki Declaration and the study was approved by the Ethics Committee, Lund University.

### 2.3. Evaluation of Motion Estimations

For each setting, two evaluation metrics for the motion estimation were calculated using 90 kernels distributed in six columns with no overlap laterally and 15 rows with 50% overlap axially. The first evaluation metric was the difference between the set displacement and the estimated displacement for each kernel. The displacements were calculated as the distance moved by each kernel between the start frame and the end frame (0.6 s after start frame) (Figure 2). The second evaluation metric was the difference between the set velocity and the estimated velocity of each kernel. The velocities were estimated as the motion between two consecutive frames 0.4 s after the start of tracking (Figure 2).

The statistical significance of changes in the mean estimation errors and standard deviations was tested for the initial length of iteration using  $k = 1$  as the reference compared to other initial lengths of iteration and cine loops sampled at a low frame rate. The statistical significance of changes in the mean estimation errors was also tested between high frame rate cine loops using  $k = 128$  as the initial length of iteration and cine loops sampled at a low frame rate. Significance testing was conducted with  $p < 0.05$  as the significance level utilizing the Analysis of Variance (ANOVA) for changes in mean values and the two-sample  $F$ -test for changes in standard deviations. Because the ANOVA was balanced and the changes in the standard deviations were limited, the unequal standard deviations were deemed to have negligible influence on the tests.

The in vivo measurements were evaluated by visual comparisons of the plotted motion estimations. One comparison was performed between ultrafast ultrasound imaging and conventional ultrasound imaging. The second comparison was performed in the same cine loop using four different positions along the artery wall.

## 3. Results

Figure 3 shows an example of lateral tracking resulting from the proposed motion estimation method for  $k = 1, 16$  and  $128$  in a high-frame cine loop. The tracking curves show that the normal frame-to-frame tracking ( $k = 1$ ) drifted away while the proposed method tracked the movement better and better with increasing  $k$ .

Figures 4 and 5 show the lateral and axial estimation errors when estimating velocity. In general, the mean estimation errors and the standard deviation decreased with increased initial length of iteration (larger  $k$ ). Increased velocity of the phantom increased the standard deviations. A smaller pitch decreased both the mean value and the standard deviation of the lateral estimation errors, while the axial estimation errors, for the most part, were unaffected. A smaller pitch was more important when using low frame rate imaging than when using high frame rate imaging.

Figures 6 and 7 show the lateral and axial estimation errors when estimating the displacement. In general, the mean estimation errors and the standard deviations decreased with increasing initial length of iteration. A smaller pitch decreased both the mean value and the standard deviation of the lateral estimation errors, while the axial estimation errors, for the most part, were unaffected.

Tables 1–4 present the estimation errors both when estimating velocity and when estimating the displacement. The lateral mean estimation error is often larger and the standard deviation is

always larger in high frame rate cine loops using frame-to-frame tracking ( $k = 1$ ) than in low frame rate cine loops ( $p < 0.05$ ). The lateral mean estimation error is often smaller and the standard deviation is usually larger in high frame rate cine loops using iterative tracking ( $k = 128$ ) than in low frame rate cine loops ( $p < 0.05$ ).

Figure 8 shows the estimated movement of the intima–media complex of the common carotid artery wall of a 47-year-old healthy female using both ultrafast ultrasound imaging ( $k = 64$ ) (solid lines) and conventional ultrasound imaging (dashed lines). The estimations in both cine loops clearly show a bi-directional longitudinal movement pattern of the same order of magnitude. The estimated movement curve, showing approximately three heartbeats, also indicates repeatability of the movement pattern. Figure 9 shows the estimated movement of the intima–media complex of the common carotid arterial wall of a 35-year-old healthy female at four different lateral positions along the vessel wall ( $k = 32$ ).

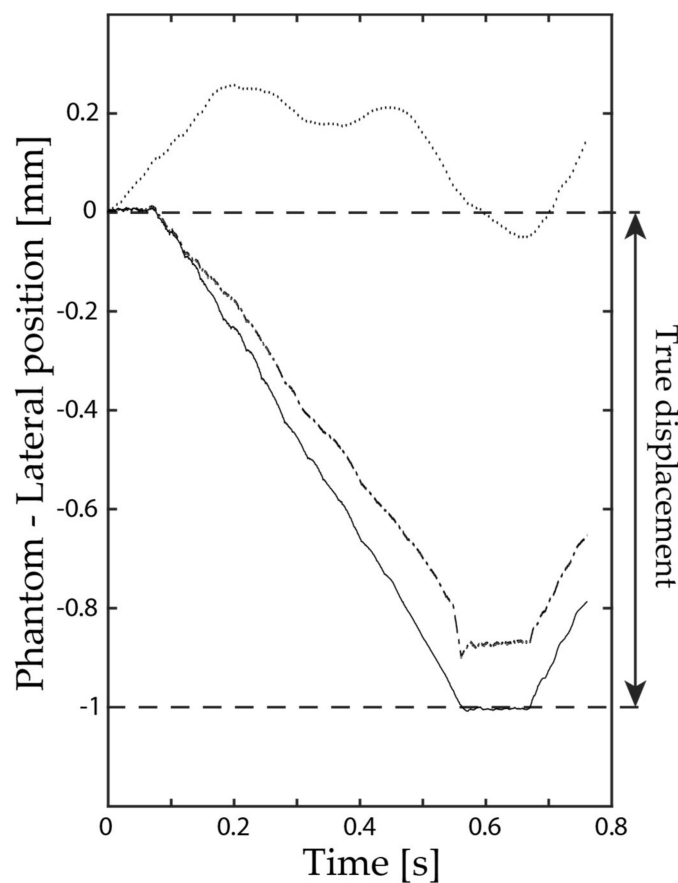


**Figure 3.** The lateral position of a kernel estimated by the proposed iterative tracking scheme with an initial length of iteration set to  $k = 128$  (solid line),  $k = 16$  (dash-dotted line), and  $k = 1$  (dotted line). The  $100\ \mu\text{m}$  pitch transducer was displaced 1 mm laterally relative to the phantom with a lateral velocity of 2 mm/s while sampling 1302 frames per second.

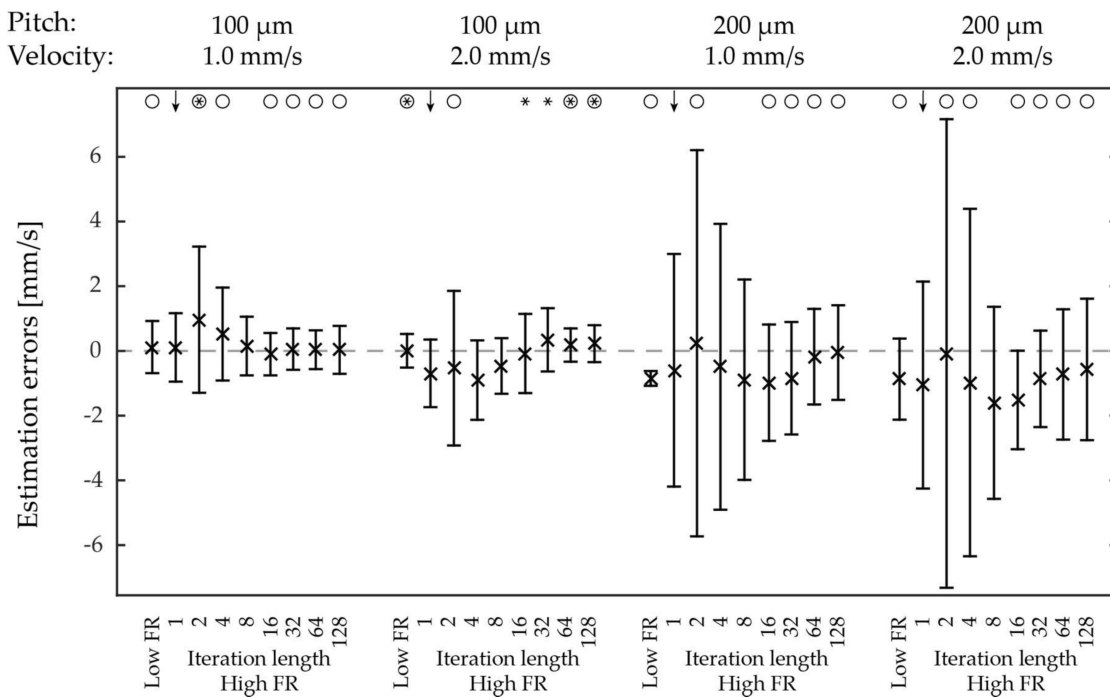


**Figure 4.** Lateral estimation errors of the velocity for two different velocities each using two different pitches (100 μm and 200 μm). The crosses indicate the mean estimation error with the error bars indicating ± one standard deviation. Significant changes ( $p < 0.05$ ) were calculated compared to  $k = 1$  in each setting (marked with an arrow). The star indicates a change in mean estimation error and a circle indicates a change in the standard deviation. FR signifies frame rate: low = 41 Hz, high = 1302 Hz.

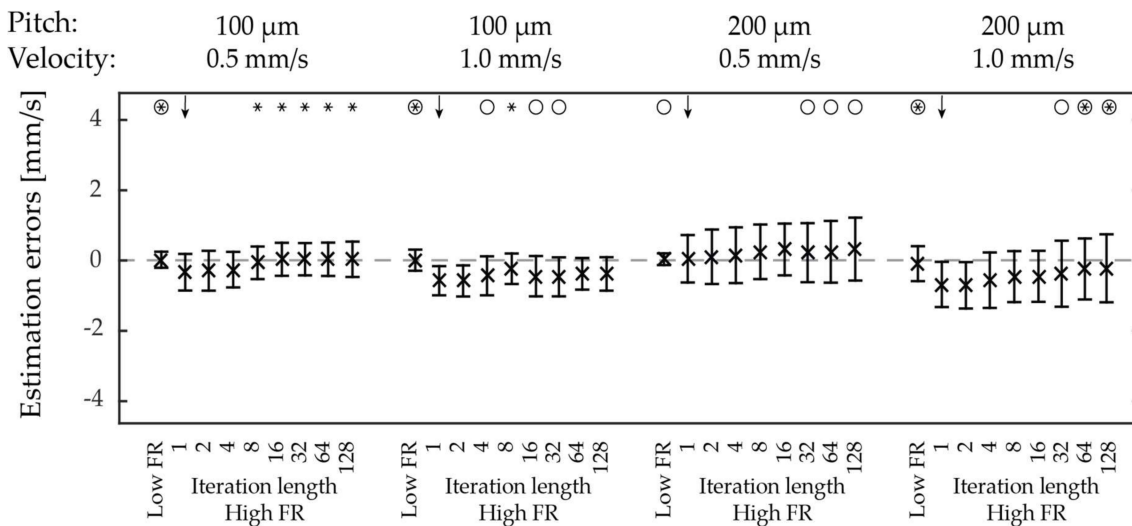


**Figure 5.** Axial estimation errors of the velocity for two different velocities each using two different pitches (100 μm and 200 μm). The crosses indicate the mean estimation with the error bars indicating ± one standard deviation. Significant changes ( $p < 0.05$ ) were calculated compared to  $k = 1$  in each setting (marked with an arrow). The star indicates a change in mean estimation error and a circle indicates a change in the standard deviation. FR signifies frame rate: low = 41 Hz, high = 1302 Hz.

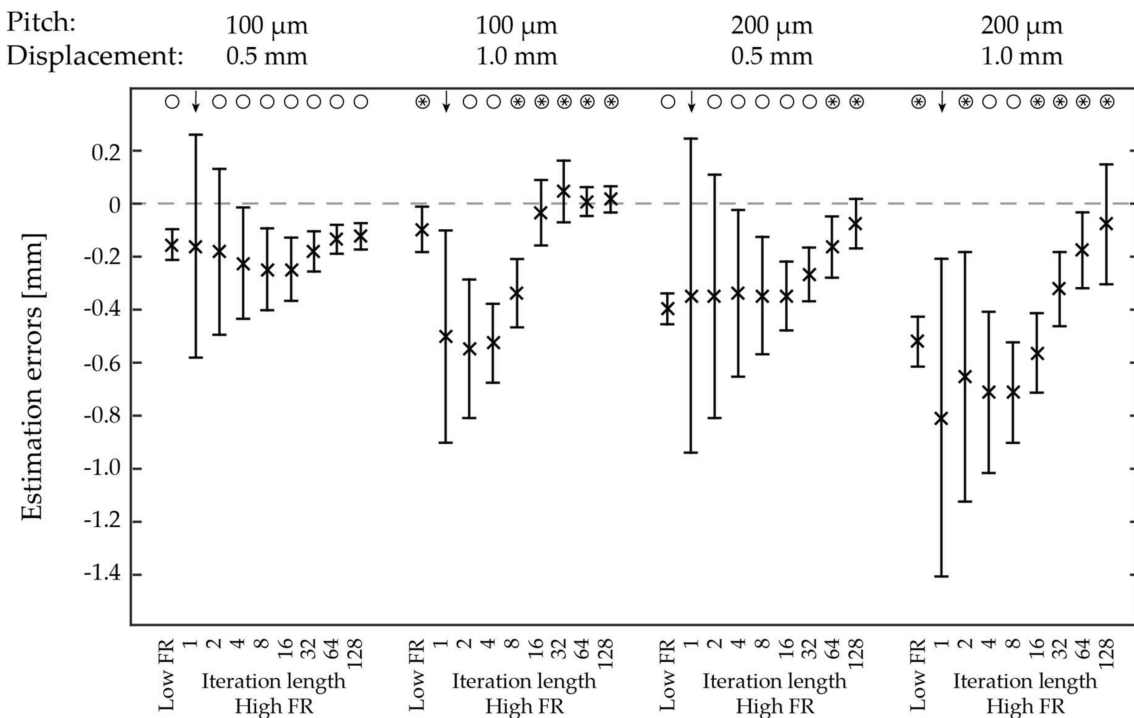


**Figure 6.** Lateral estimation errors of the displacement for two different displacements each using two different pitches (100 μm and 200 μm). The crosses indicate the mean estimation error for each setting with the error bars indicating ± one standard deviation. Significant changes ( $p < 0.05$ ) were calculated compared to  $k = 1$  in each setting (marked with an arrow). The star indicates a change in the mean estimation error and a circle indicates a change in the standard deviation. FR signifies frame rate: low = 41 Hz, high = 1302 Hz.

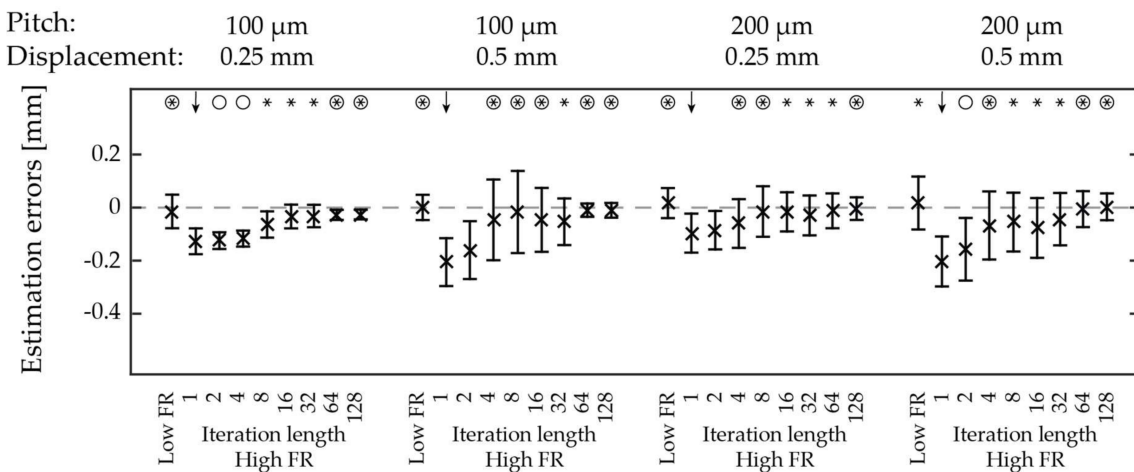


**Figure 7.** Axial estimation errors of the displacement for two different displacements each using two different pitches (100 μm and 200 μm). The crosses indicate the mean estimation error for each setting with the error bars indicating ± one standard deviation. Significant changes ( $p < 0.05$ ) were calculated compared to  $k = 1$  in each setting (marked with an arrow). The star indicates a change in the mean estimation error and a circle indicates a change in the standard deviation. FR signifies frame rate: low = 41 Hz, high = 1302 Hz.

**Table 1.** Lateral estimation errors of the velocity given as the mean estimation error  $\pm$  one standard deviation.

Pitch	100 $\mu\text{m}$	200 $\mu\text{m}$	100 $\mu\text{m}$	200 $\mu\text{m}$
Velocity	1000 $\mu\text{m/s}$	1000 $\mu\text{m/s}$	2000 $\mu\text{m/s}$	2000 $\mu\text{m/s}$
Significance	-	a, b	-	-
Low FR	117 $\pm$ 805	-852 $\pm$ 229	4 $\pm$ 520	-871 $\pm$ 1253
High FR	$k = 1$ $k = 128$	108 $\pm$ 1058 32 $\pm$ 742	-598 $\pm$ 3595 -51 $\pm$ 1462	-691 $\pm$ 1044 225 $\pm$ 570
				-1055 $\pm$ 3198 -572 $\pm$ 2184

All values are given in  $\mu\text{m/s}$ . Motion estimations were made using  $k = 128$  for the high frame rate cine loops. Significance was defined as  $p < 0.05$  in each column where a: Low frame rate (FR) vs.  $k = 1$ , b: Low frame rate (FR) vs.  $k = 128$ , and c:  $k = 1$  vs.  $k = 128$ .

**Table 2.** Axial estimation errors of the velocity given as the mean estimation error  $\pm$  one standard deviation.

Pitch	100 $\mu\text{m}$	200 $\mu\text{m}$	100 $\mu\text{m}$	200 $\mu\text{m}$
Velocity	500 $\mu\text{m/s}$	500 $\mu\text{m/s}$	1000 $\mu\text{m/s}$	1000 $\mu\text{m/s}$
Significance	a, c	a, b	-	a, c
Low FR	22 $\pm$ 228	39 $\pm$ 167	9 $\pm$ 302	-90 $\pm$ 497
High FR	$k = 1$ $k = 128$	-333 $\pm$ 502 35 $\pm$ 504	50 $\pm$ 674 324 $\pm$ 896	-576 $\pm$ 415 -381 $\pm$ 475
				-681 $\pm$ 643 -223 $\pm$ 967

All values are given in  $\mu\text{m/s}$ . Motion estimations were made using  $k = 128$  for the high frame rate cine loops. Significance was defined as  $p < 0.05$  in each column where a: Low frame rate (FR) vs.  $k = 1$ , b: Low frame rate (FR) vs.  $k = 128$ , and c:  $k = 1$  vs.  $k = 128$ .

**Table 3.** Lateral estimation errors of the set displacement given as the mean estimation error  $\pm$  one standard deviation.

Pitch	100 $\mu\text{m}$	200 $\mu\text{m}$	100 $\mu\text{m}$	200 $\mu\text{m}$
Displacement	500 $\mu\text{m}$	500 $\mu\text{m}$	1000 $\mu\text{m}$	1000 $\mu\text{m}$
Significance	-	a, b, c	b, c	a, b, c
Low FR	-154 $\pm$ 58	-397 $\pm$ 58	-97 $\pm$ 86	-521 $\pm$ 94
High FR	$k = 1$ $k = 128$	-160 $\pm$ 421 -123 $\pm$ 50	-347 $\pm$ 592 -75 $\pm$ 93	-501 $\pm$ 400 16 $\pm$ 49
				-807 $\pm$ 599 -78 $\pm$ 226

All values are given in  $\mu\text{m}$ . Motion estimations were made using  $k = 128$  for the high frame rate cine loops. Significance was defined as  $p < 0.05$  in each column where a: Low frame rate (FR) vs.  $k = 1$ , b: Low frame rate (FR) vs.  $k = 128$ , and c:  $k = 1$  vs.  $k = 128$ .

**Table 4.** Axial estimation errors of the set displacement given as the mean estimation error  $\pm$  one standard deviation.

Pitch	100 $\mu\text{m}$	200 $\mu\text{m}$	100 $\mu\text{m}$	200 $\mu\text{m}$
Displacement	250 $\mu\text{m}$	250 $\mu\text{m}$	500 $\mu\text{m}$	500 $\mu\text{m}$
Significance	a, c	a, c	a, c	a, c
Low FR	-15 $\pm$ 63	17 $\pm$ 57	1 $\pm$ 47	17 $\pm$ 100
High FR	$k = 1$ $k = 128$	-127 $\pm$ 49 -26 $\pm$ 18	-96 $\pm$ 74 -4 $\pm$ 43	-206 $\pm$ 90 -10 $\pm$ 28
				-203 $\pm$ 94 3 $\pm$ 51

All values are given in  $\mu\text{m}$ . Motion estimations were made using  $k = 128$  for the high frame rate cine loops. Significance was defined as  $p < 0.05$  in each column where a: Low frame rate (FR) vs.  $k = 1$ , b: Low frame rate (FR) vs.  $k = 128$ , and c:  $k = 1$  vs.  $k = 128$ .

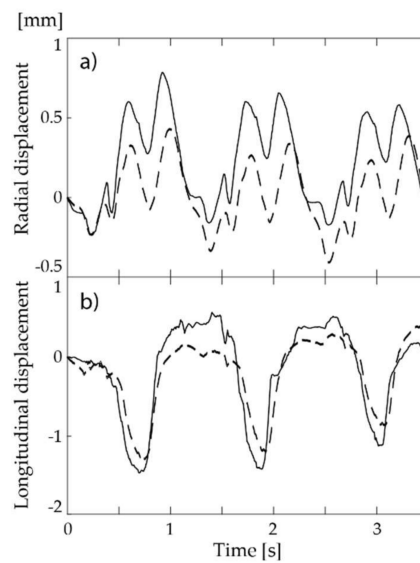


**Figure 8.** The estimated (a) radial and (b) lateral position of a kernel in vivo on the intima–media complex of the vessel wall of the common carotid artery in a healthy 47-year-old female obtained using ultrafast ultrasound imaging (solid line) and conventional ultrasound imaging (dashed line). The ultrafast ultrasound imaging was sampled at 1500 Hz and the proposed iterative tracking scheme had an initial length of iteration of  $k = 64$  frames. The conventional ultrasound imaging was sampled at 99 Hz and the tracking was frame-by-frame. The main features of the in vivo curve estimated using a high frame rate cine loop agree well with our low frame rate in vivo measurements. No ECG signal was available for synchronizing the lines and the cine loops were collected 5 minutes apart.

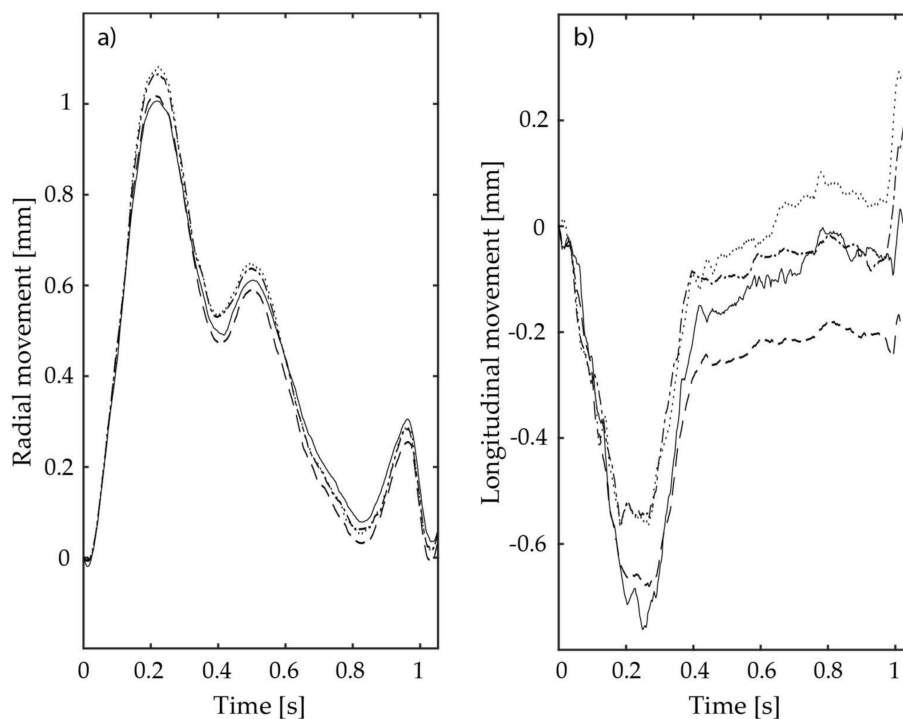


**Figure 9.** Radial movement (a) and longitudinal movement (b) of the intima–media complex of the common carotid artery wall of a healthy 35-year-old female. The kernels for the solid, dashed, dash-dot, and dotted lines were placed in order from left to right, respectively, in the first frame cine loop. The head was to the left of the image and the heart to the right. The frames were sampled at 1500 Hz and the proposed tracking scheme had an initial length of iteration of  $k = 32$  frames.

#### 4. Discussion

Frame-to-frame tracking of lateral tissue motion of the arterial wall using ultrafast ultrasound imaging is difficult as the movement per frame ( $<15\ \mu\text{m}$ ) is very small compared to the line distance (100–200  $\mu\text{m}$ ). The relative motion estimation error increases with decreasing movement per frame and the resulting movement curves become noisy and unreliable. To overcome this problem, we propose an iterative tracking scheme, with a Lagrangian viewpoint, based on temporarily down-sampling the frame-rate, anteroposterior tracking, and unbiased block-matching using two kernels per position estimate. The proposed motion estimation scheme performed well in the phantom study when estimating both velocity and displacement. The results showed increased tracking accuracy using longer initial length of iterations ( $k \geq 64$ ). The tracking performance was better using the 100  $\mu\text{m}$  pitch transducer than the 200  $\mu\text{m}$  pitch transducer. The limited in vivo study showed that the proposed 2D tissue motion estimation tracking scheme can be used in vivo and is one step towards pulse-wave velocity estimations of the longitudinal movement of the arterial wall.

As the relative motion estimation error increases with decreasing movement per frame [26], we hypothesized that it would be easier to accurately estimate a large motion than a small motion. To achieve a larger motion per frame, we used temporary down-sampling of the frame-rate. The temporary down-sampling of the frame rate also made it possible to perform anteroposterior tracking—tracking both forward and backward in the cine loop—and use two kernels per position estimate in the next iteration. The benefit of anteroposterior tracking is that bias of the motion estimate is reduced, and if the forward and the backward movements are equal, the bias is cancelled. We have previously shown that the use of an extra kernel per position reduces the mean tracking estimation errors [28]. The tracking scheme also uses much fewer estimations from the start of the tracking before reaching the investigated frame compared to frame-to-frame tracking. The combined effect of these factors is clearly shown in Figures 3, 6 and 7 as the accumulated motion estimation errors decrease with a larger initial length of iteration ( $k$ ).

In this study, both the velocity and the displacement were evaluated. The rationale is that these parameters investigate different features of a tracking method: the velocity evaluation gives an indication of the instantaneous uncertainty, whereas the displacement gives an indication of the accumulated uncertainty. In this study, the standard deviations of the velocity estimates are seemingly large. However, it should be noted that a velocity error of 1.3 mm/s corresponds to a displacement error of 1  $\mu\text{m}/\text{frame}$  (frame rate = 1302 Hz) and this is one reason why frame-to-frame tracking is likely to fail. In the evaluation, the velocity was estimated between two consecutive frames and only one estimate per kernel was used. Despite this, our proposed iterative tracking scheme based on temporarily down-sampling of the frame-rate and anteroposterior tracking enables the displacement to be accurately tracked (Figure 3, Tables 3 and 4).

Averaging of two independent sources is a common method to obtain a more robust measurement. Time-averaging over multiple frames can be performed but acts as a low-pass filter in the time domain and can hide vital information. The averaging in our method is fundamentally different in that it averages the positions of the kernels and not its movement. We achieve a more robust estimate of the position of the kernel in each frame without affecting the time resolution using an extra kernel per position estimate [28].

The signal-to-noise ratio, speckle decorrelation, out-of-plane movement, and biasing are important factors for the size of the estimation uncertainty. In ultrafast ultrasound imaging, the signal-to-noise ratio is the most important factor whereas the others mainly have an effect at larger movements per frame. We expect that the proposed tracking scheme will be affected by these factors and the size of the kernel in the same manner as other block-matching methods [26,28,31]. It is well known that larger kernel sizes give more robust motion estimations [31]. In the phantom study, we use a kernel size of  $1 \times 1\ \text{mm}^2$ , which can be regarded to be a relatively small kernel size and might explain some of the standard deviations of the motion estimations in this study. These issues need further studies.

The main finding of the phantom study is that a large length of iteration (large  $k$ ) reduces the mean estimation error and the standard deviation. However, the results are complex. Figures 4–7 show the following:

- Using a small initial length of iteration ( $k \leq 2$ ) gave rather small mean estimation errors but gave large standard deviations. Each of the motion estimations in the first iteration gave a very small error, but they accumulated to rather large errors and did so along different paths.
- Using a medium initial length of iteration ( $k = 4\text{--}32$ ) gave larger mean estimation errors but smaller standard deviations. All estimations were roughly equal, but the initial motion estimations underestimated the motions. The later iterations gave accurate estimations for the in-between frames, but their starting points from the first iteration were incorrect.
- Using a large initial length of iteration ( $k \geq 64$ ) gave small mean estimation errors and small standard deviations. The distance moved between each frame in the first iteration was large enough for the motion estimations to be accurate and for the later iterations to give accurate estimations for the in-between frames.

It could be expected that the motion estimation errors were the same when using the initial length of iteration  $k$  for a velocity  $v$  or when using  $k$  divided by 2 for a velocity two times  $v$  as the movement per frame in the initial tracking is equal. One possible explanation for the different errors, shown in Figures 6 and 7, is the fact that an estimation using  $k$  divided by two uses one iteration less than an estimation using  $k$ . Overall, as stated above, more iterations give less estimation errors in the phantom measurements; however, this issue needs further studies.

The motion estimations of the proposed tracking scheme were compared to state-of-the-art low frame rate motion estimates as this is the gold standard when estimating the longitudinal wall movement of the arterial wall [26,28,32–36]. The optimal frame rate using low frame rate imaging with a conventional linear scan scheme depends on, e.g., the signal-to-noise ratio, speckle decorrelation, out-of-plane movement, and biasing. Somewhat depending on the ultrasound scanner, we regard a frame rate of 50–90 Hz to be the optimal using a conventional linear scan scheme. Considering the large estimation errors when tracking frame-to-frame using ultrafast ultrasound imaging ( $k = 1$  in Tables 1–4), the motion estimation errors when using initial length of iteration  $k = 128$  are promising as they are of the same order of magnitude as the results using low frame rate cine loops.

The effect of using transducers with different pitch (Figures 4 and 6) was anticipated in effect if not in amplitude, i.e., tracking using a smaller pitch ( $\lambda/2$ ) gives more accurate motion estimations than using the larger pitch ( $\lambda$ ). This depends probably on both higher pixel density in the lateral direction in the resulting B-mode image and improved beamforming because of the smaller pitch. Further studies are needed to evaluate this.

The tracking performance using a low frame rate and the larger pitch was unexpectedly poor, raising the question of whether low frame rate tracking using the 200- $\mu\text{m}$ -pitch transducer can work in vivo. However, the ultrasound scanner that was used on the phantom set-up is a research scanner without, e.g., virtual scan lines, whereas the scanner we used to perform state-of-the-art tracking in vivo is a commercial ultrasound scanner utilizing virtual scan lines and many other techniques that improve the image quality. Several studies have shown that the tracking performance is sufficient when using low frame rate imaging with a conventional linear scan scheme [26,28,32–36]. The frame rate in these studies varies between 30–100 Hz.

The benefit of the implemented iterative method came not only from the use of two kernels for each estimation but also from the length of the movement between the frames in the first iteration. Considering that the initial length of iteration should be “long enough” for the best tracking accuracy and that the velocities vary drastically in in vivo measurements, it is likely that the tracking performance of the proposed tracking scheme can be optimized in vivo by using an initial length of iteration that adapts to the tissue velocity aiming to achieve the longest possible movement without significant speckle decorrelation. Potentially the best results could be achieved by using two estimations of the

movement in a cine loop: the first one determining the overall shape of the movement using a fixed frame rate, e.g., 50 Hz corresponding to  $k = 32$ , in order to maximize the initial length of iteration for each part of the cine loop; the second estimation determining the movement in all frames.

Tracking of the longitudinal movement of the arterial wall frame-to-frame using the combination block-matching and ultrafast ultrasound imaging does not work. Though no ground-truth exists, the major movement patterns in vivo using our proposed iterative tracking scheme correspond well with low frame rate motion estimates, indicating that the proposed tracking scheme could enable the study of longitudinal movement imaging of the intima–media complex using ultrafast ultrasound imaging. However, caution should be taken when drawing conclusions from these results as the magnitudes of the estimation errors on the in vivo measurements are yet unknown. In the subjects investigated, we obtained the best result using two different initial lengths of iteration ( $k = 32$  and  $64$ ). Further studies are needed to individually optimize the  $k$ .

The tracking scheme presented here is easy to implement and we believe that it can be used with most motion estimation methods with a Lagrangian viewpoint. In our implementation, the computational load is the same for any  $k$ .

There are two limitations in the phantom study. The first limitation is the chosen constant velocities of the phantom. With a maximal velocity of 2 mm/s, we are well below fast tissue motions in vivo. The second limitation is that the largest initial length of iterations was  $k = 128$ . Larger values of  $k$  were not possible to test due to the combination of using a Lagrangian viewpoint, the velocity of the phantom, and the size of the ultrasound frames. However, we do not know whether a continued increase of  $k$  will be beneficial as speckle decorrelation and out-of-plane movement can be increasingly problematic. Also, the results from the in vivo measurement (Figures 8 and 9), where  $k = 32$  and  $64$ , were optimal, indicating that the proposed tracking scheme does not necessarily continue to improve with increased  $k$  when used on in vivo measurements. Further studies, preferably with simulated data or a larger set of in vivo cine loops, are needed. Undesirable fluctuations, which are considered to be caused by pitching and yawing of the automatic stages and electrical noise in the measurement system, were contained in the estimated lateral and axial velocities. However, displacements due to such cyclic components, which are presumably caused by pitching and yawing of the automatic stages, were very small.

## 5. Conclusions

Ultrafast ultrasound imaging provides excellent time resolution of motion and enables visualization of fast processes such as the pulse wave propagation of the arterial wall. The radial pulse wave propagation has been visualized using ultrafast ultrasound imaging [14,15], but it has been more challenging to visualize the longitudinal movement and hence the propagation of the longitudinal movement of the arterial wall. A robust method for estimating 2D motions in ultrafast ultrasound cine loops is needed for estimation of the longitudinal movement, and here we have presented a tracking scheme that might fill that role. The phantom evaluation clearly shows that our tracking scheme reduced the accumulated errors. In addition, the limited in vivo study shows that the major movement patterns in vivo correspond well with low frame rate motion estimates, indicating that the proposed tracking scheme could enable the study of longitudinal movement of the intima–media complex using ultrafast ultrasound imaging, and is one step towards estimating the propagation velocity of the longitudinal movement of the arterial wall.

**Author Contributions:** J.A., H.T. and M.C. were involved in the design of the new method, J.A., H.H. and M.C. conceived and designed the experiments; H.H., J.A., Å.R.A., M.C. performed the experiments; J.A. analyzed the data; J.A., Å.R.A. and M.C. interpreted the results, H.H., E.B. and A.R. contributed with instrumentation and instrumentation knowledge; J.A. wrote the paper; All authors approved the final draft of the manuscript.

**Acknowledgments:** We thank Ann-Kristin Jönsson for skillful technical assistance and The Swedish Research Council, the Swedish Foundation for International Cooperation in Research and Higher Education (STINT), the Medical and Technical Faculties, Lund University, and the Skåne County Council's Research and Development Foundation for funding.

**Conflicts of Interest:** The authors declare no conflict of interest. The founding sponsors had no role in the design of the study; in the collection, analyses, or interpretation of data; in the writing of the manuscript, and in the decision to publish the results.

## References

- Gennisson, J.-L.; Provost, J.; Deffieux, T.; Papadacci, C.; Imbault, M.; Pernot, M.; Tanter, M. 4-D Ultrafast Shear-Wave Imaging. *IEEE Trans. Ultrason. Ferroelectr. Freq. Control* **2015**, *62*, 1059–1065. [[CrossRef](#)] [[PubMed](#)]
- Bercoff, J.; Chaffai, S.; Tanter, M.; Sandrin, L.; Catheline, S.; Fink, M.; Gennisson, J.L.; Meunier, M. In Vivo Breast Tumor Detection using Transient Elastography. *Ultrasound Med. Biol.* **2003**, *29*, 1387–1396. [[CrossRef](#)]
- Muller, M.; Gennisson, J.-L.; Deffieux, T.; Tanter, M.; Fink, M. Quantitative Viscoelasticity Mapping of Human Liver using Supersonic Shear Imaging: Preliminary in Vivo Feasibility Study. *Ultrasound Med. Biol.* **2009**, *35*, 219–229. [[CrossRef](#)] [[PubMed](#)]
- Tanter, M.; Bercoff, J.; Sandrin, L.; Fink, M. Ultrafast Compound Imaging for 2-D Motion Vector Estimation: Application to Transient Elastography. *IEEE Trans. Ultrason. Ferroelectr. Freq. Control* **2002**, *49*, 1363–1374. [[CrossRef](#)] [[PubMed](#)]
- Palmeri, M.L.; Wang, M.H.; Dahl, J.J.; Frinkley, K.D.; Nightingale, K. Quantifying Hepatic Shear Modulus in Vivo using Acoustic Radiation Force. *Ultrasound Med. Biol.* **2008**, *34*, 546–558. [[CrossRef](#)] [[PubMed](#)]
- Hansen, P.M.; Olesen, J.B.; Pihl, M.J.; Lange, T.; Heerwagen, S.; Pedersen, M.M.; Rix, M.; Lönn, L.; Jensen, J.A.; Nielsen, M.B. Volume Flow in Arteriovenous Fistulas using Vector Velocity Ultrasound. *Ultrasound Med. Biol.* **2014**, *40*, 2707–2714. [[CrossRef](#)] [[PubMed](#)]
- Lenge, M.; Ramalli, A.; Boni, E.; Liebgott, H.; Cachard, C.; Tortoli, P. High-frame-rate 2-D vector blood flow imaging in the frequency domain. *IEEE Trans. Ultrason. Ferroelectr. Freq. Control* **2014**, *61*, 1504–1514. [[CrossRef](#)] [[PubMed](#)]
- Takahashi, H.; Hasegawa, H.; Kanai, H. Echo speckle imaging of blood particles with high-frame-rate echocardiography. *Jpn. J. Appl. Phys.* **2014**, *53*, 07KF08. [[CrossRef](#)]
- Deffieux, T.; Jean-Luc, G.; Tanter, M.; Fink, M. Assessment of the Mechanical Properties of the Musculoskeletal System Using 2-D and 3-D Very High Frame Rate Ultrasound. *IEEE Trans. Ultrason. Ferroelectr. Freq. Control* **2008**, *55*, 2177–2190. [[CrossRef](#)] [[PubMed](#)]
- Errico, C.; Osmanski, B.-F.; Pezet, S.; Couture, O.; Lenkei, Z.; Tanter, M. Transcranial functional ultrasound imaging of the brain using microbubble-enhanced ultrasensitive Doppler. *NeuroImage* **2016**, *124*, 752–761. [[CrossRef](#)] [[PubMed](#)]
- Tong, L.; Gao, H.; Choi, H.F.; D’hooge, J. Comparison of Conventional Parallel Beamforming With Plane Wave and Diverging Wave Imaging for Cardiac Applications: A Simulation Study. *IEEE Trans. Ultrason. Ferroelectr. Freq. Control* **2012**, *59*, 1654–1663. [[CrossRef](#)] [[PubMed](#)]
- Hasegawa, H.; Kanai, H. High-frame-rate echocardiography using diverging transmit beams and parallel receive beamforming. *J. Med. Ultrason.* **2011**, *38*, 129–140. [[CrossRef](#)] [[PubMed](#)]
- Hasegawa, H.; Kanai, H. Simultaneous imaging of artery-wall strain and blood flow by high frame rate acquisition of RF signals. *IEEE Trans. Ultrason. Ferroelectr. Freq. Control* **2008**, *55*, 2626–2639. [[CrossRef](#)] [[PubMed](#)]
- Salles, S.; Chee, A.J.Y.; Garcia, D.; Yu, A.C.H.; Vray, D.; Liebgott, H. 2-D Arterial Wall Motion Imaging Using Ultrafast Ultrasound and Transverse Oscillations. *IEEE Trans. Ultrason. Ferroelectr. Freq. Control* **2015**, *62*, 1047–1058. [[CrossRef](#)] [[PubMed](#)]
- Kruizinga, P.; Mastik, F.; van den Oord, S.C.H.; Schinkel, A.F.L.; Bosch, J.G.; de Jong, N.; van Soest, G.; van der Steen, A.F.W. High-Definition Imaging of Carotid Artery Wall Dynamics. *Ultrasound Med. Biol.* **2014**, *40*, 2392–2403. [[CrossRef](#)] [[PubMed](#)]
- Nichols, W.W.; O’Rourke, M.F. *McDonald’s Blood Flow in Arteries*, 6th ed.; Edward Arnold: London, UK, 2011.
- Blacher, J.; Guerin, A.P.; Pannier, B.; Marchais, S.J.; Safar, M.E.; London, G.M. Impact of aortic stiffness on survival in endstage renal disease. *Circulation* **1999**, *99*, 2434–2439. [[CrossRef](#)] [[PubMed](#)]
- Cinthio, M.; Ahlgren, Å.R.; Bergkvist, J.; Jansson, T.; Persson, H.W.; Lindström, K. Longitudinal movements and resulting shear strain of the arterial wall. *Am. J. Physiol. Heart. Circ. Physiol.* **2006**, *291*, H394–H402. [[CrossRef](#)] [[PubMed](#)]
- Nilsson, T.; Ahlgren, Å.R.; Jansson, T.; Persson, H.W.; Nilsson, J.; Lindström, K.; Cinthio, M. A method to measure shear strain with high-spatial-resolution in the arterial wall non-invasively in vivo by tracking zerocrossings of B-Mode intensity gradients. In Proceedings of the 2010 IEEE Ultrasonics Symposium (IUS), San Diego, CA, USA, 11–14 October 2010; pp. 491–494.

20. Idzenga, T.; Holewijn, S.; Hansen, H.H.G.; de Korte, C.L. Estimating Cyclic Shear Strain in the Common Carotid Artery Using Radiofrequency Ultrasound. *Ultrasound Med. Biol.* **2012**, *38*, 2229–2237. [[CrossRef](#)] [[PubMed](#)]
21. Zahnd, G.; Boussel, L.; Serusclat, A.; Vray, D. Intramural shear strain can highlight the presence of atherosclerosis: A clinical in vivo study. In Proceedings of the 2011 IEEE International Ultrasonics Symposium (IUS), Orlando, FL, USA, 18–21 October 2011; pp. 1770–1773.
22. Ahlgren, Å.R.; Cinthio, M.; Steen, S.; Nilsson, T.; Sjöberg, T.; Persson, H.W.; Lindström, K. Longitudinal displacement and intramural shear strain of the porcine carotid artery undergo profound changes in response to catecholamines. *Am. J. Physiol. Heart. Circ. Physiol.* **2012**, *302*, H1102–H1115. [[CrossRef](#)] [[PubMed](#)]
23. Zahnd, G.; Maple-Brown, L.J.; O’Dea, K.; Moulin, P.; Celermajer, D.S.; Skilton, M.R.; Vray, D.; Sérusclat, A.; Alibay, D.; Bartold, M.; et al. Longitudinal displacement of the carotid wall and cardiovascular risk factors: Associations with aging, adiposity, blood pressure and periodontal disease independent of cross-sectional distensibility and intima-media thickness. *Ultrasound Med. Biol.* **2012**, *38*, 1705. [[CrossRef](#)] [[PubMed](#)]
24. Svedlund, S.; Eklund, C.; Robertsson, P.; Lomsky, M.; Gan, L.-M. Carotid artery longitudinal displacement predicts 1-year cardiovascular outcome in patients with suspected coronary artery disease. *Arterioscler. Thromb. Vasc. Biol.* **2011**, *31*, 1668–1674. [[CrossRef](#)] [[PubMed](#)]
25. Svedlund, S.; Gan, L.-M. Longitudinal common carotid artery wall motion is associated with plaque burden in man and mouse. *Atherosclerosis* **2011**, *217*, 120–124. [[CrossRef](#)] [[PubMed](#)]
26. Albinsson, J.; Ahlgren, Å.R.; Jansson, T.; Cinthio, M. A combination of parabolic and grid slope interpolation for 2D tissue displacement estimations. *Med. Biol. Eng. Comput.* **2017**, *55*, 1327–1338. [[CrossRef](#)] [[PubMed](#)]
27. Hasegawa, H. Phase-Sensitive 2D Motion Estimators Using Frequency Spectra of Ultrasonic Echoes. *Appl. Sci.* **2016**, *6*, 195. [[CrossRef](#)]
28. Albinsson, J.; Brorsson, S.; Ahlgren, Å.R.; Cinthio, M. Improved Tracking Performance of Lagrangian Block-Matching Methodologies using Block Expansion in the Time Domain—In silico, phantom and in vivo evaluations using ultrasound images. *Ultrasound Med. Biol.* **2014**, *40*, 2508–2520. [[CrossRef](#)] [[PubMed](#)]
29. Boni, E.; Bassi, L.; Dallai, A.; Guidi, F.; Ramalli, A.; Ricci, S.; Housden, J.; Tortoli, P. A reconfigurable and programmable FPGA-based system for nonstandard ultrasound methods. *IEEE Trans. Ultrason. Ferroelectr. Freq. Control* **2012**, *59*, 1378–1385. [[CrossRef](#)] [[PubMed](#)]
30. Tortoli, P.; Bassi, L.; Boni, E.; Dallai, A.; Guidi, F.; Ricci, S. An Advanced Open Platform for ULtrasound Research. *IEEE Trans. Ultrason. Ferroelectr. Freq. Control* **2009**, *56*, 2207–2216. [[CrossRef](#)] [[PubMed](#)]
31. Friemel, B.H.; Bohs, L.N.; Trahey, G.E. Relative performance of two-dimensional speckle-tracking techniques: Normalized correlation, non-normalized correlation and sum-absolute-difference. *Proc. IEEE Ultrason.* **1995**, *2*, 1481–1484.
32. Cinthio, M.; Ahlgren, Å.R.; Jansson, T.; Eriksson, A.; Persson, H.W.; Lindström, K. Evaluation of an ultrasonic echo-tracking method for measurements of arterial wall movements in two dimensions. *IEEE Trans. Ultrason. Ferroelectr. Freq. Control* **2005**, *52*, 1300–1311. [[CrossRef](#)] [[PubMed](#)]
33. Cinthio, M.; Ahlgren, Å.R. Intra-Observer Variability of Longitudinal Movement and Intramural Shear Strain Measurements of the Arterial Wall using Ultrasound Non-Invasively in vivo. *Ultrasound Med. Biol.* **2010**, *36*, 697–704. [[CrossRef](#)] [[PubMed](#)]
34. Zahnd, G.; Boussel, L.; Marion, A.; Durand, M.; Moulin, P.; Serusclat, A.; Vray, D. Measurement of Two-Dimensional Movement Parameters of the Carotid Artery Wall for Early Detection of Arteriosclerosis: A Preliminary Clinical Study. *Ultrasound Med. Biol.* **2011**, *37*, 1421–1429. [[CrossRef](#)] [[PubMed](#)]
35. Numata, T.; Hasegawa, H.; Kanai, H. Basic study on detection of outer boundary of arterial wall using its longitudinal motion. *Jpn. J. Appl. Phys.* **2007**, *46*, 4900–4907. [[CrossRef](#)]
36. Yli-Ollila, H.; Laitinen, T.; Weckström, M.; Laitinen, T.M. Axial and radial waveforms in Common Carotid Artery: An advanced method for studying arterial elastic properties in ultrasound imaging. *Ultrasound Med. Biol.* **2013**, *39*, 1168–1177. [[CrossRef](#)] [[PubMed](#)]

